This Article is under Formatting, the PDF's ready file will be replaced soon.

International Journal of Machine Systems and Manufacturing

Technology
Article type: Review
Volume: 4, Issue: 1
Received Date: 14 January 2026
Accepted Date: 27 February 2026
Published Date: 12 March 2026

Development and implementation of Solar-Thermoelectric Hybrid Energy Harvester

Anish Kumar[1], Praveen Kumar choudhary[2]
[1]Assistant Professor, Department of Mechanical engineering, BIT, Sindri, Jharkhand, India.
[2]Reseach Scholar, Department of Mechanical engineering. EIT Faridabad, India.

Email : roniesomadder@gmail.com

Abstract -
In today's consumer-oriented and technology-driven market, researchers are increasingly emphasizing the need to harvest energy from ambient and renewable sources to support sustainable power generation and to minimize dependence on conventional energy resources such as batteries and fossil-fuel-based electricity. The rising deployment of portable electronics, wireless sensor networks, and Internet of Things (IoT) devices has created an urgent demand for compact, low-power, long-life, and maintenance-free energy solutions. In many real-world scenarios, frequent battery replacement is impractical due to high cost, limited accessibility, and environmental concerns related to battery disposal. Hence, ambient energy harvesting has emerged as a promising approach for enabling self-powered electronic systems.

Energy harvesting techniques provide enormous potential by converting naturally available energy such as human motion, mechanical vibrations, thermal gradients, airflow, and other waste energy into usable electrical output. Generally speaking, energy harvesters are transducers that take in energy from their surroundings and transform it into electrical power that may be stored or used directly.Among various harvesting mechanisms, triboelectric and thermoelectric energy harvesting methods are considered highly advantageous due to their simple structure, lightweight configuration, scalability, and suitability for small-scale applications.

This research focuses on the practical implementation and performance validation of Thermoelectric Energy Harvesting (THEH) using a developed hardware prototype and experimental test setup. A usable amount of electrical energy is generated under realistic operating conditions, and the output parameters are measured, analyzed, and validated to assess feasibility for real-time applications. The obtained results confirm that triboelectric and thermoelectric based harvesting can be an effective solution for powering low-power electronics and self-sustaining sensing systems in future smart applications.

Keywords : DC-DC boost converter, generator system, TEG modules, thermocouple, STEG

.

1. Introduction

The low-power electronic devices and portable devices always need a continuous power supply which is usually fulfilled by batteries. To minimize the use of battery power supply for these devices, discovering new renewable energy sources has become a key area of research. These renewable energy harvesting methods are able to utilize the untapped surrounding ambient energy from the environment and can persuasively address above issues. Many techniques such as thermoelectricity, piezoelectricity, pyroelectricity, photovoltaic, triboelectricity etc. are studied broadly to understand the capturing and efficient harnessing of energy from these ambient sources. Another development for maximum utilization of available energy sources is hybrid integrated systems. Many such techniques are available which combines two or more sources in single integrated system for co-power generation. Among the listed technologies, a thermoelectric energy harvester/generator can capture spontaneously available thermal energy from sunrays, power plants, vehicles and pavements to generate electrical energy by Seebeck effect [8]. A semiconductor-based thermocouple can be employed to generate electrical energy from thermal energy provided a requisite temperature gradient is maintained constantly. These thermocouples are available in the form of commercially available modules with ceramic outer covering. In the absence of any moving part for energy generation these light-weight modules offer various advantages like noiseless, robustness and larger shelf-life. Various compositional and structural exploration for the fabrication of semiconductors with small band gap, provided new and efficient thermocouple materials for further examination.

In last few decades researchers have shown greater interest in efficient utilization of solar energy for electricity generation. Few attempts have been made to elevate the contributions of thermal energy in sunlight for harnessing useable energy some high-performance coatings for enhanced heat absorption. Ample amount of heat available from sunlight can easily operate the thermoelectric modules by creating a temperature difference/gradient required for corresponding thermal heat conversion. Association of solar-thermal effect together for power generation have seen plenty of promising applications like heating of water, electricity generation, water distillation etc. [9-11]. One study integrated carbon materials with bismuth telluride modules using carbon nanotube–based composites featuring a nanostructured architecture, achieving approximately 1% output efficiency under ambient sunlight. Another work designed

and analyzed a solar thermoelectric generator (STEG) that delivered an output power of 0.91 W with a maximum attainable efficiency of 2.21% when operated within a vacuum enclosure.

A flat-panel type STEG was later demonstrated with a peak efficiency of 4.6%, which was further enhanced through the application of optical concentration techniques. In a separate development, a thermoelectric generator employing a PMMA Fresnel lens system for heat concentration achieved a reported efficiency of 51.33%, generating 1.08 W of power under matched load conditions at the output side.

Carbon nanotubes and graphene oxide are examples of zero band gap materials that can be employed to improve the performance of thermal-based energy harvesting methods. They increase the capacity of heat absorption by the surface of thermoelectric device to elevate their performance. Candle soot with high carbon content is a well-known cost-effective source for carbon nanoparticle fabrication. It displays superhydrophobic property and gives stable results even at 500^{o} C [1]. In the visible light spectrum, deposition of candle soot on the surface exhibits favourable properties such as luminescence [14]. When concentrated sunlight is directed onto highly absorbent materials, the generated output power increases significantly. One study reported a 50-fold enhancement in harvested energy using a candle-soot–coated PZT pyroelectric device, while another demonstrated a 17-fold improvement through diesel exhaust soot coating. In a related approach, a carbon-based double-layer solar–thermal structure was proposed to localize heat effectively for steam generation.

For efficient thermoelectric generator (TEG) operation, maintaining an optimal temperature difference across the module and ensuring matched load impedance are essential. Maximum power transfer occurs when the load resistance equals the internal resistance of the TEG. To facilitate battery charging, one investigation connected three TEG modules to a microcontroller-controlled SEPIC DC–DC converter. Another study reported TEG arrays achieving 80% efficiency using buck–boost converters for improved load conductance. A maximum power point tracking (MPPT)–based TEG system with synchronous rectification was also developed, capable of transferring 47 W to a load. Additionally, a SEPIC converter was employed in a separate design to charge a Li-ion battery using a single TEG module.

measured a boosted voltage of 47.54 V across a 10F capacitor for a temperature difference of 56^{o}C. In this work, we designed a cost-effective answer for substantial enhancement in thermoelectric energy harvesting. We exposed the upper surface of

thermoelectric module (TEC-12706) to a candle flame multiple times for better heat absorption by the black body. The required temperature difference was maintained using concentrated solar radiations and regular water flow to obtain better electrical output. The voltage was further increased using a dc-dc boost converter. To demonstrate the energy storage capability of the system we also charged a 2.4V VARTA NI-MH rechargeable battery from the generated amplified voltage [1-10].

2. System design

A thermoelectric module (TEC-12706) is the first component of the suggested system, which is a thermoelectric energy harvesting system. 2) Coating of candle soot 3) A 784 cm2 Fresnel lens, and 4) A water block. The solar radiations were used for heating upper surface of TEG and water block provided flowing cold water for cooling the other side. The TEC1-12706 Thermoelectric module with dimensions 40mm x 40mm x 3.9 mm is used which is based on Al_2O_3 material. Other specifications of the selected module are listed in Table 2.1.

Table 2.1. Specifications of TEC1-12706

Parameter	Value
Dimensions (mm)	40 x 40 x 4.2
Weight (grams)	17
Resistance (Ω)	0.85
No. of thermocouples	127
Max. Current (Amps)	6.4
Max. Voltage (Volts)	14.4
Max. Power (Watts)	40
Max. Temperature difference, ΔT (°C)	68
Hot side temperature (°C)	80

Before irradiating sunlight, the thermoelectric module was exposed to direct flame of candle to coat the layer of carbon soot on the upper surface.

3. Experimental

A mechanical structure assembly was placed to grasp the lens at desired position to maximize the focussed sun rays. Along with continuous heating from top, the TEG was

placed on an aluminium water block to maintain the temperature difference by cooling the bottom surface [11-15].

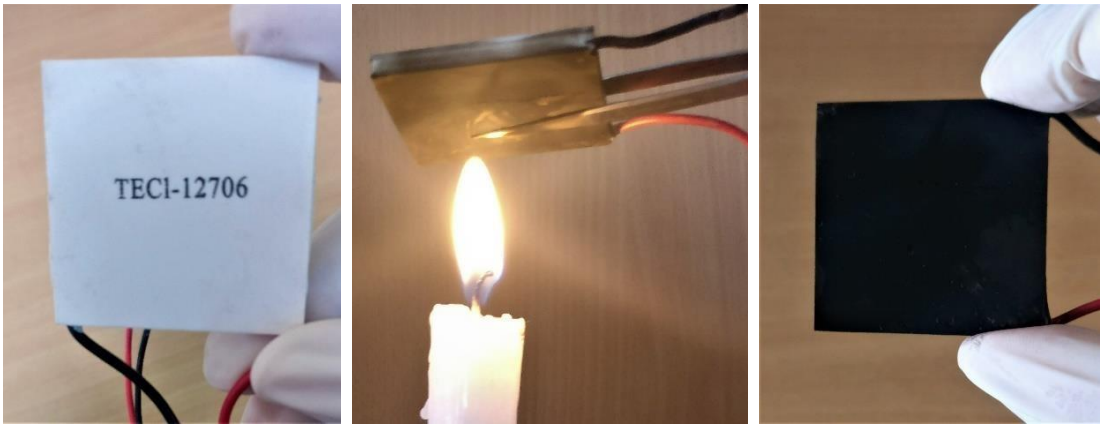

(a) **(b)** **(c)**

Fig. 2.1. Candle-soot Coating process (a) Uncoated TEG module (b) Soot coating process (c) Carbon soot coated TEG module

Fig. 2.3. shows an electrical DC-DC boost converter circuit for raising the voltage obtained from TEG to further charge a 2.4 V battery. The basic design consists of the following components:

Schottky diode, D (BAT86)

A 30 mH inductor (L),

A 4.7 µF capacitor (C_L)

and a 2N7000 MOSFET switch (S).

In ideal conditions above lossless components will generate an output voltage V_{out} categorized by the duty cycle of the MOSFET switching speed. The output voltage V_{out} is given by equation 2.1 below:

$$Vout = \frac{Vi}{1-d} \qquad (2.1)$$

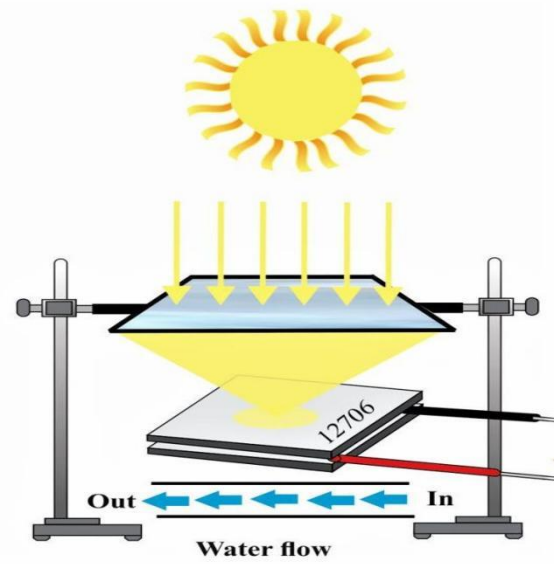

Fig. 2.2. Schematic of thermoelectric generator system

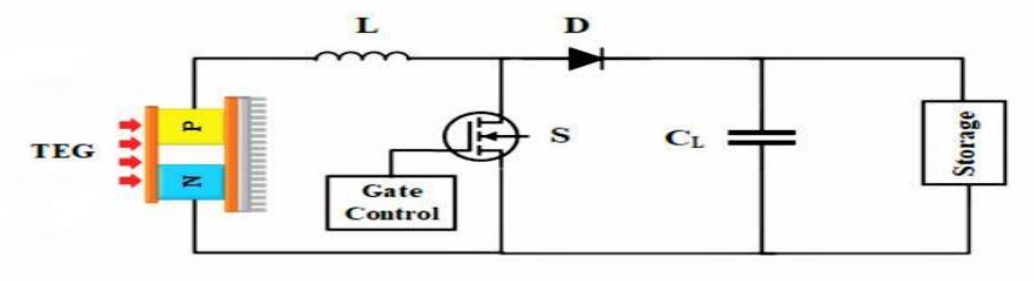

Fig. 2.3. DC-DC boost converter

The duty cycle, *d* can be varied using a PWM method in which the fixed width of a pulse, *Ton,* is changed instantaneously.

The high-speed switching MOSFETs controls the swift ON-OFF switching time and thereby regulates the output voltage level. The electrical parameters of the thermoelectric generator are measured to analyse the system performance. A 50Ω resistor was connected at the load side to record the open-circuit voltage (V_{oc}), output load current (I), cold-side temperature (T_c) and hot-side temperature (T_h) using following instruments [16-30]:

1. Electronic logging meter, Fluke 287, for recording the output current and voltage.
2. A K-Type thermocouple for recording hot and cold-side temperatures.
3. A common submersible pump for garden usage that circulates water in a water block.

Table 2.2. below gives the range and accuracies of the above listed instruments.

Table 2.2. Accuracies of the measuring instruments

Instrument	Parameter	Accuracy	Range
Fluke logging meter	DC current	0.05%	500µA-10A
	DC voltage	0.025%	50mA-1000V
Thermocouple	Temperature in ºC	+/- 2.2°C	-40 to 260°C

4. Results and discussion

The XRD pattern shown in Fig. 4.4. was obtained using a Cu-K based Rigaku diffractometer with a 9-kW rotating anode to uniquely characterise the CS coated surface of the module.

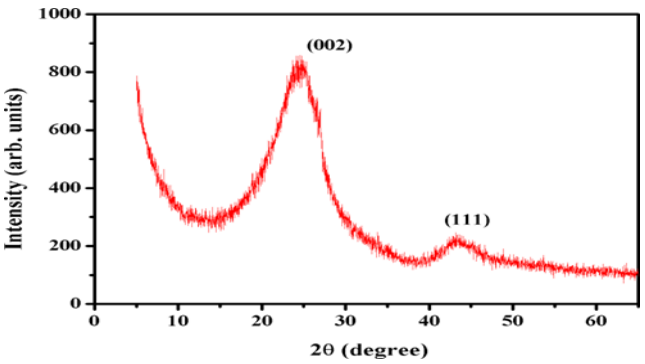

Fig. 4.4. XRD pattern of carbon soot coated thermoelectric module

The presence of amorphous carbon material is confirmed by the visible high intensity peak at 24.6° 2θ position. Another low intensity broad peak seen at 43.16° 2θ position indicates the presence of low-quality carbon particles [31-40]. These results correspond to the reported findings during characteristics study of carbon nanoparticles present in candle

wax, kerosene and diesel [16-17]. The peaks appearing at 24.6° and 43.16° correspond to hexagonal (graphite) structure for (002) and (111) planes of carbon particles respectively. Fig. 4.5(a) shows the Raman spectrum of incident light and The soot particles' absorption of visible, near-infrared, and ultraviolet light is seen in Fig. 4.5(b).

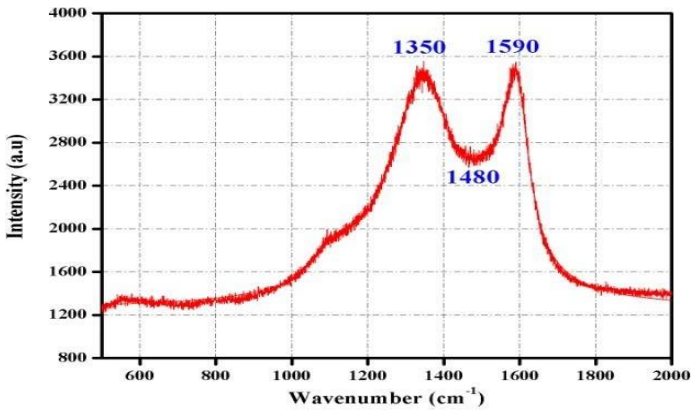

(a)

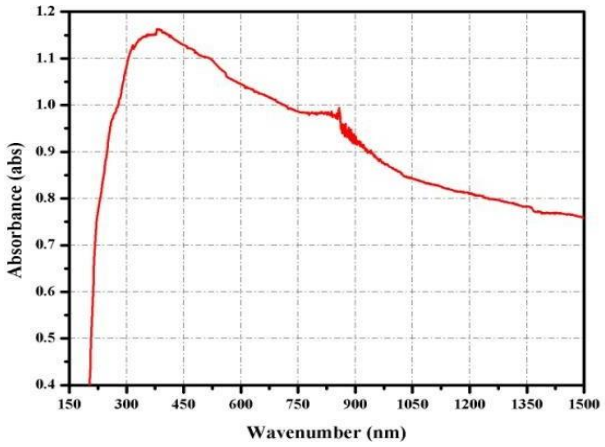

(b)

Fig. 4.5. Spectrum graphs (a) Raman Spectrum
(b) NIR-UV-Visible spectrum of carbon soot coated thermoelectric module

The Raman spectrum provides details on how light is scattered by the vibrations of the irradiation molecules, highlighting information about the crystal lattice. A typical 535 nm green laser from HORIBA, Model: Lab Ram Hr Evolution, was used to irradiate the coated module at a grating rate of 1800 lines per millimetre. At room temperature, the intensity of dispersed wavelength was measured in relation to the wave number (1/wavelength) in the range of 100–2000 cm-1. The presence of projecting peaks is consistent with the intensity fluctuations predicted by several carbon-based vibration mode structures.The peak at 1350 cm-1 is caused by amorphous carbon, structural flaws, and sp3-hybridized carbon. The existence of sp2 orientated C-C stretched bonds in soot causes another peak to arise at 1590 cm-1. Certain disordered quantities of carbon material present in soot are linked to the weaker Raman band at 1480 cm-1. For the spectrum range of 2400-1200 nm, which falls in the NIR region, a gradual increase in absorbance value was observed. The absorption value in the NIR-UV region between 1200-370 nm increased noticeably when compared to the region below 370 nm, where it decreased rapidly. According to scanning electron micrographs, the diameter of carbon particles ranges from 30 to 40 nm (not shown here) [41-55]. Fig. 4.6. shows the open- circuit voltage generated from TEG for uncoated and coated samples from L0 to L4.

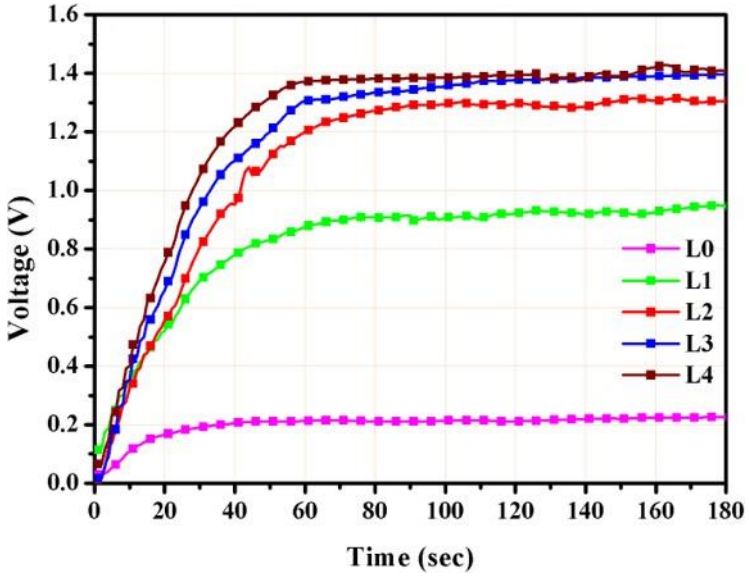

Figure 4.6. Open-circuit TEG output voltage

Because of the consistent rise in temperature differential between the two sides of the four-times-coated module, the L4 sample unquestionably produced the best results. Up to the fourth coating, the temperature differential grew before declining. The temporal temperature differential is determined by the amount of heating that reaches the

thermoelectric material. As the candle soot thickness rose, the thermoelectric sample surface could not be able to absorb heat, which would reduce the output voltage.While the uncoated module L0 could only provide 0.22 V, the voltage in the L4 sample increases dramatically to 1.46 V. Compared to the uncoated sample, the open circuit voltage across the four-times-coated sample increases more than six times more quickly. The amount of heat applied to all of the coated and uncoated samples is a major factor in this increase. The findings also show that the coated thermoelectric module had a much higher load current than the untreated sample [56-60].

Fig. 4.7. below shows the current across 50Ω load resistor.

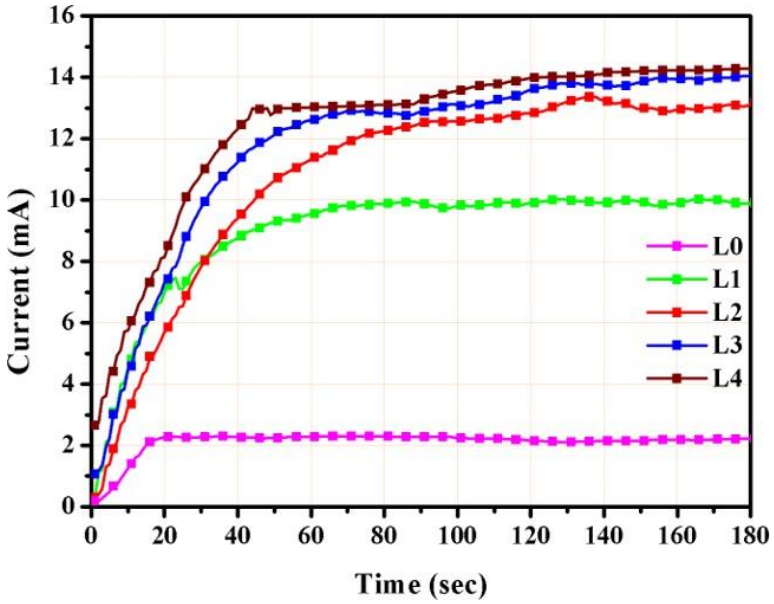

Fig. 4.7. Load current from TEG

While the uncoated module (L0) could only produce 2.2 mA across the load by applying constant heating and cooling on both sides of the module, a maximum short-circuit current of 14.2 mA was observed utilising the L4 sample [61-70]. Due to the strong heat absorption across four times the candle-soot coated sample, an astonishing rise of more than six times the uncoated module value was seen. The graphs for the output power obtained by the uncoated and coated samples over a load resistance of 50 Ω following sequential 180 seconds of heating and cooling are displayed in Fig. 4.8. The temperature gradient graph for the uncoated and coated samples over the two sides of the thermoelectric module is shown in Fig. 4.9.The L4 sample produced a maximum power of 10.2 mW with a maximum current of 14.2 mA, but the uncoated TEG module had a lower output power of 0.24 mW. When compared to uncoated modules, this indicates a significant increase of over 42 times by four times coated modules. Candle-

soot coated TEG modules clearly perform better than normal uncoated modules by producing noticeably greater electrical outputs.

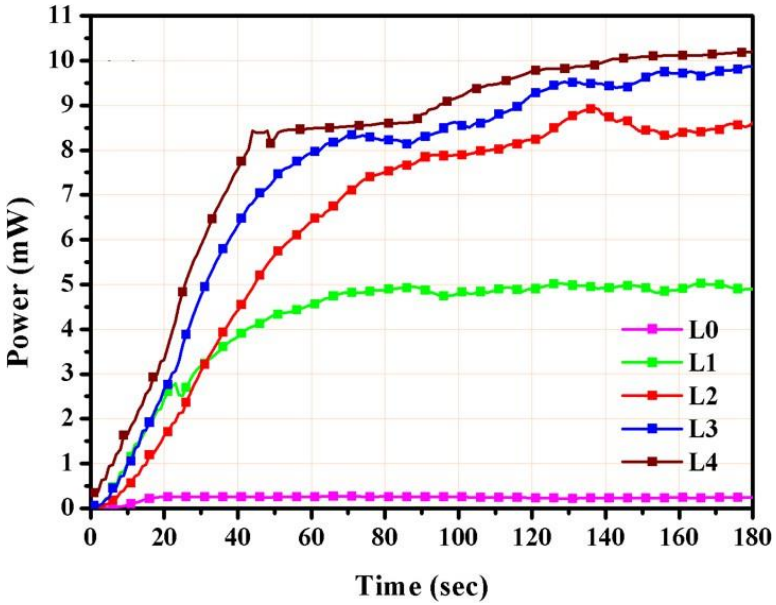

Fig. 4.8. Output power from TEG

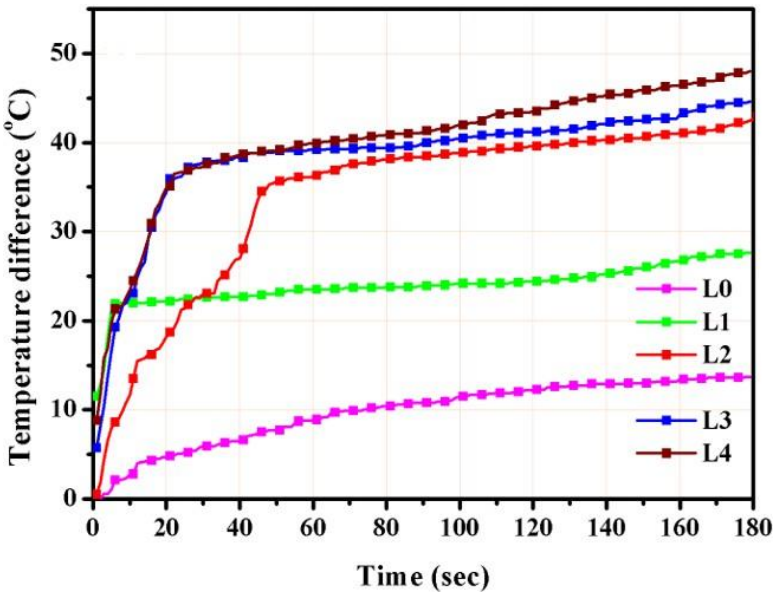

Fig. 4.9. Temperature gradient of TEG

Figure 4.10 displays a comparison of the TEG output voltage, current, and associated temperature differential measurements for uncoated and coated samples over a 60-second period. Four layers of carbon soot on the thermoelectric cell provide the greatest open-circuit voltage, as shown in Fig. 4.10(a), whereas other lower coated samples produce a lower voltage value. All of the coated samples show a noticeable rise in voltage when compared to the untreated samples.As the number of soot layers increased the corresponding maximum output voltage also increased. As evident from the plots

even the L1 sample (single coat module) showed a remarkable increase in the output voltage being generated from a conventional TEG cell.

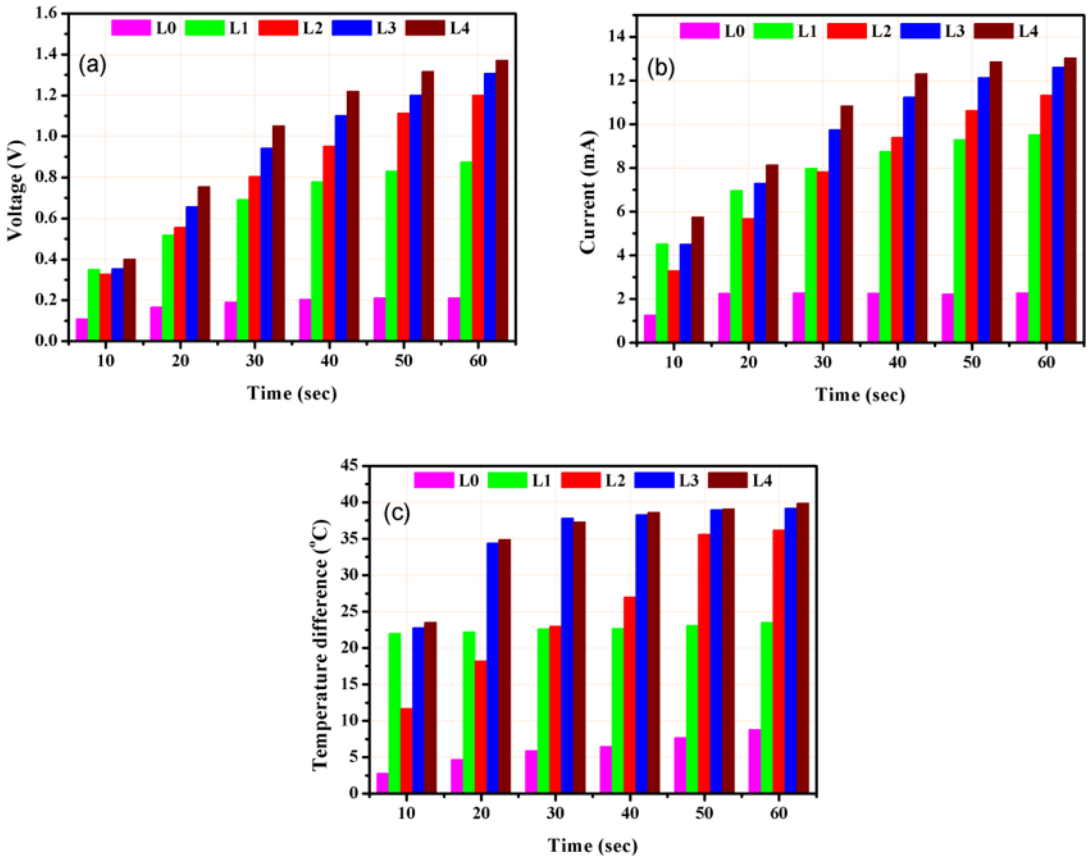

Fig. 4.10. TEG electrical outputs (a) Open-circuit voltage (b) Short-circuit current and (c) Temperature difference

With further consecutive layers of carbon soot the voltage increased with each coated layer till the fourth layer. The results from further soot layers were not recorded as the voltage began to decrease after four layers of carbon coating. Similarly, the short-circuit current values are shown in Fig. 4.10(b) as recorded for L4 and other samples. When compared to other cases under consideration the current also rises with each consecutive layer of carbon soot coating. A remarkable increase in current value was recorded after first soot layer as compared to output current from uncoated cell. This sequential increase in output voltage and current values was credited to gradual corresponding increase in the temperature difference. The plots from Fig. 4.10(c) shows the temperature gradient created on two sides of uncoated and coated samples to increase the electrical outputs. The corresponding recorded values for open-circuit voltage, short-circuit load current and the temperature difference generated across TEG are listed in Table 4.3. The maximum voltage reaches 1.37 V when recorded for first

60 seconds of system operation.

Table 4.3. Voltage and current obtained for corresponding temperature difference L0- No coating, L1- One coat, L2- Two coats, L3- Three coats, L4- Four coats

Time (sec)	Voltage (V)					Current (mA)					Temperature difference (oC)				
	L0	L1	L2	L3	L4	L0	L1	L2	L3	L4	L0	L1	L2	L3	L4
10	0.11	0.35	0.33	0.35	0.40	1.27	4.52	3.30	4.51	5.77	2.8	22.0	11.7	22.8	23.5
20	0.17	0.52	0.56	0.66	0.75	2.27	6.97	5.69	7.30	8.14	4.7	22.2	18.2	34.4	34.9
30	0.19	0.69	0.80	0.94	1.05	2.28	7.98	7.83	9.76	10.84	5.9	22.6	23.0	37.8	37.3
40	0.21	0.78	0.95	1.10	1.22	2.27	8.76	9.41	11.24	12.32	6.5	22.7	27.0	38.3	38.6
50	0.21	0.83	1.11	1.20	1.32	2.24	9.29	10.63	12.13	12.86	7.7	23.1	35.6	39.0	39.1
60	0.21	0.88	1.20	1.31	1.37	2.28	9.53	11.32	12.61	13.03	8.8	23.5	36.2	39.2	39.9

To show the effectiveness of the system to successfully convert the thermal energy to electrical energy the conversion efficiency of the system was calculated. Fig. 4.11. shows the energy conversion efficiency plot of the system under consideration. The efficiency was calculated using equations 4.3.-4.6. The value of Seebeck coefficient (α) required for efficiency calculations was calculated for uncoated cell and all the coated cells individually. The efficiency readings for all the candle-soot coated samples (L1-L4) showed a significant increase as compared to the efficiency of uncoated sample. The efficiency readings for all the candle-soot coated samples (L1-L4) showed a significant increase as compared to the efficiency of uncoated sample. The average temperature difference created across the uncoated cell was 9.8^{o}C with a maximum temperature difference of 13.8^{o}C. The average temperature gradient of 40.3^{o}C was achieved across the L4 coated sample with a maximum value reaching 48^{o}C.

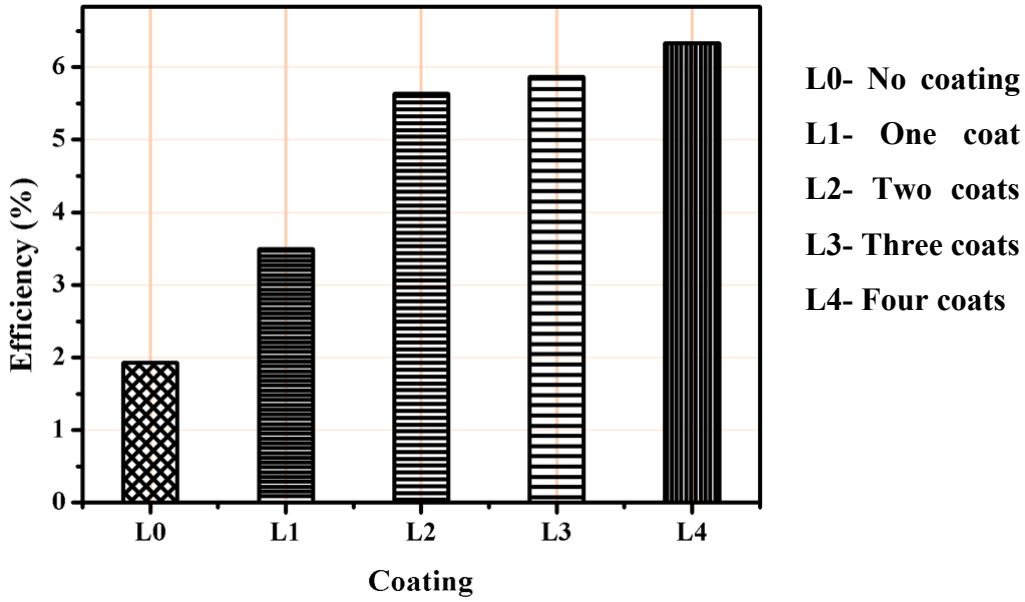

Fig. 4.11. Maximum energy conversion efficiency

As evident from the graph the efficiency of the system was maximum when integrated with four soot layers coated thermoelectric module. A maximum conversion efficiency of 6.3% was achieved by the system for converting the heat energy from sun to electrical energy. This performance was recorded by the corresponding temperature difference of 48ºC at the end of 180 seconds by L4 sample. It was observed that the uncoated cell showed 1.9% conversion efficiency for a maximum temperature gradient of 13.8ºC. Looking at the results for other coated modules, L1, L2 and L3 give maximum efficiency of 3.5%, 5.6% and 5.9% respectively. The results clearly showed that coating the cells with carbon material -based candle soot layer enhanced the overall system efficiency by 4.4%. The additional layer of soot for enhanced heat absorption made the system almost four times more efficient as compared to conventional uncoated cell-based thermoelectric system. A DC-DC boost converter was used to increase the 1.46 V output voltage from L4 in order to charge a 2.4 V rechargeable VARTA battery in order to assess the system's energy storage capacity. By periodically energising a 30 mH inductor, the output was increased to a little higher value of 2.4 V to charge a 4.7 µF capacitor.

Table 5.4. Comparative analysis of thermoelectric generators

Ref	Thermometric Module	No. of Modules	Coating	Concentrator	Heating source	Open-circuit voltage (V)	Current (mA)	Power (mW)	Efficiency (%)
Lin et al. 218	NA	1	Cu NPs@Zn foil, Ck@membrane, RGO@Ni foam	-	Xenon lamp	0.21	1.34	0.28	NA
Sudharsh an et al. 219	NA	3	Al alloy	Glass plate	Solar radiations	0.8	55.25	44.2	0.82
Ogbonna ya et.al.149	1261G-7L31-04CQ	1	Nickel-tin coating on Cu plate	-	Halogen lamp	0.13	70.38	9.15	NA
Köysal et al. 137	TEG1-12611-8.0	2	Graphene	Fresnel lens	Solar radiations	1.41	193.61	273	0.6
Sundarra j et al. 220	TEG1-127- 1.4-1.0	6	-	Parabolic trough collector	Three 50W electrical heater	5.7	810	4700	1.2

5. Conclusion

This chapter presents an experimental investigation of using a thermoelectric module covered with candle soot to harvest thermoelectric energy. A temperature differential was produced between two of the module's surfaces by focussing sunlight and moving water. The module was coated with different thicknesses of candle soot using a candle flame and the crystal morphology was examined using Raman spectroscopy. When coated with the fourth consecutive CS layer, a maximum of 1.46 V of open-circuit voltage and 14.2 mA of peak current are obtained. This is a significant improvement over a conventional (uncoated) thermoelectric module, which has a maximum voltage of 0.22V and a peak current of 2.2 mA. The 10.2 mW harvested power from soot coated TEG is reported to outperform the conventional uncoated module with 0.24 mW power only. This technique also yields an electrical conversion efficiency of 6.3 percent. A rechargeable battery is also charged in 1.5 hours to illustrate the energy storage application. Low and ultra-low power sensors, as well as other electronic equipment, can be powered by the stored energy. By cascading many TEG modules, the harnessed output power may be further boosted. Nonetheless, the impedance matching of such a setup may be examined for maximum power transmission.

6. References

1. M. J. Aberuee, E. Baniasadi and M. Ziaei-Rad, “Performance analysis of an integrated solar based thermo-electric and desalination system,” Applied Thermal Engineering, vol. 110, pp. 399–411, 2017.
2. K.S. Ong, M.S. Naghavi and C. Lim, “Thermal and electrical performance of a hybrid design of a solar-thermoelectric system,” Energy Conversion and Management, vol. 133, pp. 31-40, 2017.
3. J.D. Park, H. Lee and M. Bond, “Uninterrupted thermoelectric energy harvesting using temperature-sensor-based maximum power point tracking system,” Energy Conversion and Management, vol. 86, pp. 233-240, 2014.
4. Y. Köysal, A. E. Özdemir and T. Atalay, “Experimental and modeling study on solar system using linear Fresnel lens and thermoelectric module,” Journal of Solar Energy Engineering, vol. 140, no. 6, pp. 061003, 2018.
5. M.H. Nia, A.A. Nejad, A.M. Goudarzi, M. Valizadeh and P. Samadian, “Cogeneration solar system using thermoelectric module and fresnel lens,” Energy

Conversion and Management, vol. 84, pp. 305-310, 2014.

6. P. Cheruvu, V.P. Kumar and H.C. Barshilia, “Experimental analysis and evaluation of a vacuum enclosed concentrated solar thermoelectric generator coupled with a spectrally selective absorber coating,” International Journal of Sustainable Energy, vol. 37, no. 8, pp. 782-798, 2018.

7. D. Kraemer et al., “High-performance flat-panel solar thermoelectric generators with high thermal concentration,” Nature materials, vol. 10, no. 7, pp. 532-538, 2011.

8. P.C. Dias, F.J.O Morais, M.B. de Morais França, E.C. Ferreira, A. Cabot and J.A.S. Dias, “Autonomous multisensor system powered by a solar thermoelectric energy harvester with ultralow-power management circuit,” IEEE Transactions on Instrumentation and Measurement, vol. 64, no. 11, pp. 2918-2925, 2015.

9. P. Carvalhaes-Dias, A. Cabot and J.A. Siqueira Dias, “Evaluation of the thermoelectric energy harvesting potential at different latitudes using solar flat panels systems with buried heat sink,” Applied Sciences, vol. 8, no. 12, pp. 2641, 2018.

10. J. He, Y. Liu and R. Funahashi, “Oxide thermoelectrics: The challenges, progress, and outlook,” Journal of Materials Research, vol. 26, no. 15, pp. 1762–1772, 2011.

11. M. Rull-Bravo, A. Moure, J. F. Fernández and M. Martín-González, “Skutterudites as thermoelectric materials: revisited,” RSC Advances, vol. 5, no. 52, pp. 41653–41667, 2015.

12. Z. Yang, J. PradoGonjal, M. Phillips, S. Lan, A. Powell, P. Vaqueiro, M. Gao, R. Stobart and R. Chen, “Improved thermoelectric generator performance using high temperature thermoelectric materials,” SAE Technical Series, no. 2017-01-0121, 2017.

13. Y.J. Zeng, D. Wu, X.-H. Cao, W.-X. Zhou, L.-M. Tang and K.-Q. Chen, “Nanoscale organic thermoelectric materials: Measurement, theoretical models, and optimization strategies,” Advanced Functional Materials, vol. 30, no. 8, pp. 1903873, 2020.

14. M. Ibáñez, Z. Luo, A. Genc, L. Piveteau, S. Ortega, D. Cadavid, O. Dobrozhan, Y. Liu, M. Nachtegaal, M. Zebarjadi and J. Arbiol, “High-performance thermoelectric nanocomposites from nanocrystal building blocks,” Nature Communication, vol. 7, no. 1, pp. 10766, 2016.

15. C. Cho, K. L. Wallace, P. Tzeng, J.-H. Hsu, C. Yu and J. C. Grunlan, “Outstanding low temperature thermoelectric power factor from completely organic thin films enabled by multidimensional conjugated nanomaterials,” Advanced Energy Materials, vol. 6, no. 7, pp. 1502168, 2016.

16. H. Jin, J. Li, J. Iocozzia, X. Zeng, P.C. Wei, C. Yang, N. Li, Z. Liu, J.H. He, T. Zhu and J. Wang, “Hybrid organic-inorganic thermoelectric materials and devices,” Angew. Chem. Int. Ed Engl., vol. 58, no. 43, pp. 15206–15226, 2019.

17. J. Yu, H. Wang, L. Kong, H. Zhu and Q. Zhu, “Study on the Thermal Conductivity of Mannitol Enhanced by Graphene Nanoparticles for Thermoelectric Power Generation,” Journal of Nanomaterials, 2020.

18. E. Ogbonnaya, A. Gunasekaran and L. Weiss, “Micro solar energy harvesting using thin film selective absorber coating and thermoelectric generators,” Microsystem Technologies, vol. 19, no. 7, pp. 995–1004, 2013.

19. Y. Deng, W. Zhu, Y. Wang and Y. Shi, “Enhanced performance of solar-driven photovoltaic– thermoelectric hybrid system in an integrated design,” Solar Energy, vol. 88, pp. 182–191, 2013.

20. E. Escobar, M. Diaz and J. C. Zagal, “Evolutionary design of a satellite thermal control system: Real experiments for a CubeSat mission,” Applied Thermal Engineering, vol. 105, pp. 490–500, 2016.

21. C.J. Liang, J.D. Liao, A.J. Li, C. Chen, H.Y. Lin, X.J. Wang and Y.H. Xu, “Relationship between wettabilities and chemical compositions of candle soots,” Fuel, vol. 128, pp. 422-427, 2014.

22. G. E. J. Poinern, S. Brundavanam, M. Shah, I. Laava and D. Fawcett, “Photothermal response of CVD synthesized carbon (nano) spheres/aqueous nanofluids for potential application in direct solar absorption collectors: a preliminary investigation,” Nanotechnology, science and applications, vol. 5, 2012.

23. B.C. Martindale, G.A. Hutton, C.A. Caputo and E. Reisner, “Solar hydrogen production using carbon quantum dots and a molecular nickel catalyst,” Journal of the American Chemical Society, vol. 137, no. 18, pp. 6018-6025, 2015.

24. P. Azad, V.P. Singh and R. Vaish, “Candle soot-driven performance enhancement in pyroelectric energy conversion,” Journal of Electronic Materials, vol. 47, no. 8, pp. 4721-4730, 2018.

25. P. Azad, M. Sharma and R. Vaish, “Diesel Exhaust Emission Soot Coated Pyroelectric Materials for Improved Thermal Energy Harvesting,” Global Challenges, vol. 3, no. 6, pp. 1800089, 2019.

26. G. Karalis, L. Tzounis, E. Lambrou, L.N. Gergidis and A.S. Paipetis, “A carbon fiber thermoelectric generator integrated as a lamina within an 8-ply laminate epoxy composite: Efficient thermal energy harvesting by advanced structural materials,” Applied Energy, vol. 253, pp. 113512, 2019.

27. H. Ghasemi, G. Ni, A.M. Marconnet, J. Loomis, S. Yerci, N. Miljkovic and G. Chen, “Solar steam generation by heat localization,” Nature Communication, vol. 5, no. 1, pp. 4449, 2014.

28. R. Hu, B.A. Cola, N. Haram, J.N. Barisci, S. Lee, S. Stoughton, G. Wallace, C. Too, M. Thomas,

A. Gestos and M.E.D. Cruz, “Harvesting waste thermal energy using a carbon-nanotube-based thermo-electrochemical cell,” Nano Letters, vol. 10, no. 3, pp. 838–846, 2010.

29. J. Eakburanawat and I. Boonyaroonate, “Development of a thermoelectric battery charger with microcontroller-based maximum power point tracking technique. Applied Energy, vol. 83, no. 7,
pp. 687-704, 2006.

30. H. Nagayoshi and T. Kajikawa, “Mismatch power loss reduction on thermoelectric generator systems using maximum power point trackers,” 25th International Conference on Thermoelectrics,
pp. 210-213, 2006.

31. L. Chen, D. Cao, Y. Huang and F.Z. Peng, “Modeling and power conditioning for thermoelectric generation,” IEEE Power Electronics Specialists Conference, pp. 1098-1103, 2008.

32. C. E. Kinsella, S. M. O’Shaughnessy, M. J. Deasy, M. Duffy and A. J. Robinson, “Battery charging considerations in small scale electricity generation from a thermoelectric module,” Applied Energy, vol. 114, pp. 80–90, 2014.

33. P. Azad, “Temperature Controlled Voltage Regulated Boost Converter for thermoelectric Energy Harvesting,” IETE Journal of Research, pp.1-8, 2019.

34. Q. Liu, X. Wu, M. Zhao, L. Wang and X. Shen, “30–300mV input, ultra low power, self-startup DC-DC boost converter for energy harvesting system,” IEEE Asia Pacific Conference on Circuits and Systems, pp. 432-435, 2012

35. P. H. Chen, C. S. Wu and K. C. Lin, “A 50 nW-to-10 mW output power tri-mode digital buck converter with self-tracking zero current detection for photovoltaic energy harvesting,” IEEE Journal of Solid-State Circuits, vol. 51, no. 2, pp. 523–532, 2016.

36. H. Yu, M. Chen, C. Wu, K.T. Tang and G. Wang, “A batteryless and single inductor DC-DC boost converter for thermoelectric energy harvesting application with 190mV cold-start voltage,” IEEE International Symposium on Circuits and Systems, pp. 1-4, 2018.

37. M. Hammerle, M. Haynes, and S. Mcneil, “Use of automatic vehicle location and passenger count data to evaluate bus operations: experience of the Chicago Transit Authority, Illinois,” Transportation Research Record, vol. 1903, no. 1, pp. 27–34, 2005.

38. Z. Yang and L. S. C. Pun-Cheng, “Vehicle detection in intelligent transportation systems and its applications under varying environments: A review,” Image and Vision Computing, vol. 69, pp. 143–154, 2018.

39. E. Frontoni, A. Mancini, R. Pierdicca, M. Sturari and P. Zingaretti, “Analysing human movements at mass events: A novel mobile-based management system based on active beacons and AVM,” 24th Mediterranean Conference on Control

and Automation , pp. 605-610, 2016.

40. M. K. H. Majumdar, H. Biswas, M. H. A. Shaim and K. T. Ahmmed, "Automated energy saving and safety system," International Conference on Electrical Engineering and Information & Communication Technology, pp. 1-6, 2014.

41. G. Waradkar, H. Ramina, V. Maitry, T. Ansurkar, A. Rawat and M. P. Das, "Automated room light controller with visitor counter," Imperial Journal of Interdisciplinary Research, vol. 2, no. 4, pp. 777–780, 2016.

42. B. Shajahan, "ARM Based Electronic Notice Board through Zigbee with Room Lights Control using PIR Sensor," 2014.

43. B.N. Naik, M.M. Reddy, S. Kanungo and S.S. Kar, "Speed detection device in road traffic accidents: A realistic approach in India!", Journal of family medicine and primary care, vol. 5, no. 3, pp. 741, 2016.

44. A. Van Niekerk, S. Suffla and M. Seedat, "Crime, Violence and Injury Prevention in South Africa: Developments and Challenges, Medical Research Council-University of South Africa Crime," Violence and Injury Lead Programme, Johannesburg: Psychological Society of South Africa, pp. 8- 22, 2004.

45. O.V. Schoor, J.L.V. Niekerk and B. Grobbelaar, "Mechanical failures as a contributing cause to motor vehicle accidents—South Africa," Accident Analysis & Prevention, vol. 33, pp. 713-21, 2001.

46. R. R Tiwari and G. B Ganveer, "A Study on Human Risk Factors in Non-fatal Road Traffic accidents at Nagpur," Indian Journal of Public Health, vol. 52, no. 4, pp. 197-199, 2008.

47. R. Elvik, R. Christensen and A. Amundsen, "Speed and road accidents. An evaluation of the Power Model", TØI report, pp. 740, 2004.

48. Z.L. Wang, "Triboelectric nanogenerators as new energy technology and self-powered sensors– Principles, problems and perspectives," Faraday discussions, vol. 176, pp. 447-458, 2015.

49. M. Ha, J. Park, Y. Lee and H. Ko, "Triboelectric generators and sensors for self-powered wearable electronics," ACS Nano, Vol. 9, no. 4, pp. 3421-7 2015,

50. F. Invernizzi, S. Dulio, M. Patrini, G. Guizzetti and P. Mustarelli, "Energy harvesting from human motion: materials and techniques," Chemical Society Reviews, vol. 45, no. 20, pp. 5455-73, 2016.

51. P. Azad and R. Vaish, "Portable triboelectric based wind energy harvester for low power applications," European Physical Journal - Plus, vol. 132, no. 6, pp. 253, 2017.

52. Y.A. Badamasi, "The working principle of an Arduino," IEEE International Conference on Electronics, Computer and Computation, pp. 1-4, 2014.

53. D. Yadav and P. Azad, “Design and implementation of robust low cost and low power prototype for generic counting system,” IEEE International Conference on Computing, Communication and Automation, pp. 1493-1498, 2017.

54. P. Chaudhary and P. Azad, P., “Demonstration of double electrode vertical-sliding triboelectric generator,” IEEE International Conference on Computing, Communication and Automation, pp. 1483-1487, 2017.

55. Khushboo and P. Azad, “Triboelectric Nanogenerator based on Vertical Contact Separation Mode for Energy Harvesting,” IEEE International Conference on Computing, Communication and Automation, pp. 1499-1501, 2017.

56. B. W. Cook, S. Lanzisera and K. S. J. Pister, “SoC Issues for RF Smart Dust,” IEEE, vol. 94, no. 6, pp. 1177–1196, 2006.

57. P. D. Mitcheson, E. M. Yeatman, G. K. Rao, A. S. Holmes and T. C. Green, “Energy harvesting from human and machine motion for wireless electronic devices,” IEEE, vol. 96, no. 9, pp. 1457– 1486, 2008.

58. T. Torfs, V. Leonov, C. Van Hoof and B. Gyselinckx, “Body-heat powered autonomous pulse oximeter,” IEEE Conference on Sensors, pp. 427-430, 2006.

59. N. M. Pletcher, S. Gambini and J. M. Rabaey, “A 2GHz 52µW wake-up receiver with -72dBm sensitivity using uncertain-IF architecture,” IEEE Jornal of Solid-State Circuits, vol. 44, no. 1, pp. 269-280, 2008.

60. F. Zhang, Y. Zhang, J. Silver, Y. Shakhsheer, M. Nagaraju, A. Klinefelter, J. Pandey, J. Boley, E. Carlson, A. Shrivastava and B. Otis, “A batteryless 19µW MICS/ISM-Band energy harvesting body sensor node SoC for ExG applications,” IEEE Journal of Solid-State Circuits, vol. 48, no. 1, pp. 199–213, 2012.

61. Y.S. Lin, D. Sylvester and D. Blaauw, “An ultra low power 1V, 220nW temperature sensor for passive wireless applications,” IEEE Custom Integrated Circuits Conference, pp. 507-510, 2008.

62. R.J.M. Vullers, R. van Schaijk, I. Doms, C. Van Hoof and R. Mertens, “Micropower energy harvesting,” Solid-State Electronics, vol. 53, no. 7, pp. 684-693, 2009.

63. J.D. Prades, R. Jimenez-Diaz, F. Hernandez-Ramirez, S. Barth, A. Cirera, A. Romano-Rodriguez,
S. Mathur and J.R. Morante, “Ultralow power consumption gas sensors based on self-heated individual nanowires,” Applied Physics Letters, vol. 93, no. 12, pp. 123110, 2008.

64. M. Kishi, H. Nemoto, T. Hamao, M. Yamamoto, S. Sudou, M. Mandai and S. Yamamoto, “Micro thermoelectric modules and their application to wristwatches as an energy source,” International Conference on Thermoelectrics, pp. 301-307, 2003.

65. R. Ambrosi, H. Williams and P. Samara-Ratna, “Americium-241 radioisotope thermoelectric generator development for space applications”, 2013.

66. J. Lofy and L. E. Bell, “Thermoelectrics for environmental control in automobiles,” International Conference on Thermoelectrics, pp. 471-476, 2003.

67. J. Lagrandeur, D. Crane and A. Eder, “Vehicle fuel economy improvement through thermoelectric waste heat recovery,” in DEER conference, pp. 1–24, 2005.

68. J. C. Bass, N. B. Elsner and F. A. Leavitt, “Performance of the 1 kW thermoelectric generator for diesel engines,” in AIP Conference Proceedings, vol. 316, no. 1, 295-298, 1994.

69. R. Y. Nuwayhid, D. M. Rowe and G. Min, “Low cost stove-top thermoelectric generator for regions with unreliable electricity supply,” Renewable Energy, vol. 28, no. 2, pp. 205–222, 2003.

70. F. Frobenius, G. Gaiser, U. Rusche and B. Weller, “Thermoelectric generators for the integration into automotive exhaust systems for passenger cars and commercial vehicles,” Journal of Electronic Materials, vol. 45, no. 3, pp. 1433–1440, 2016.